Simulation of homogeneous and inhomogeneous shear turbulence

By Javier Jiménez†

1. Motivation and objectives

Homogeneous sheared turbulence has been used as an intermediate stage of complication between the simple isotropic case and inhomogeneous flows such as channels and free shear layers (Champagne *et al.* 1970; Tavoularis & Karnik 1989). The idea is that it should contain some of the basic mechanisms of shear flows, such as non-zero tangential Reynolds stresses and production of turbulent kinetic energy, while avoiding the complication of more realistic cases. Rotation of the frame of reference can be included without abandoning homogeneity; the resulting balance of the roughly opposing effects of shear and rotation has also been the subject of extensive study. However, although such approximations are useful, their limitations have to be understood whenever they are applied to a new problem. The shear and the angular rotation velocity impose a time scale on homogeneous turbulent flows, but their only intrinsic length scale is due to viscosity, which can hopefully be neglected when the Reynolds number is high enough. This means that such flows cannot reach a universal long-term statistically steady state, since such a state would necessarily have a definite length scale. If a steady state is reached, it has to be dominated by either the initial or the boundary conditions.

Systems in which a steady state is forced by the boundaries, or by other artificial means, have sometimes been studied in the hope that their shortest scales retain some universal characteristics independent of the details of the larger structures (Pumir 1996). The latter, however, are necessarily subject to the limitations just mentioned, complicating the interpretation of their long-term behavior.

Consider again the question of the integral length scale, or equivalently of the velocity scale. Characteristic lengths, for example, must either increase without bound, decrease, or stay proportional to those of the initial conditions. In the first case, the flow eventually collides with any outer length imposed by the experimental or numerical conditions. In the second one, viscosity eventually dominates, and the fluctuations decay. The third case, if it existed, would be interesting in that it would introduce the possibility of multiple turbulent basins of attraction, unconnected with each other and controlled by the initial conditions. It would however be roughly equivalent to the cases in which the scale is fixed by the experimental domain. A fourth case, in which the integral length wanders chaotically in time without any fixed characteristic value, is also possible in principle, but in practice the integral length would eventually become large or small enough to interfere with either the viscous or the outer experimental scales, making this case equivalent to the first or second possibilities.

An especially interesting acse arises in the context of the evolution of astrophysical accretion disks, which, within a certain approximation, can be represented locally as a homogeneous box with a particular ratio of rotation to shear. The problem was reviewed

† School of Aeronautics, Universidad Politécnica, 28040 Madrid, Spain

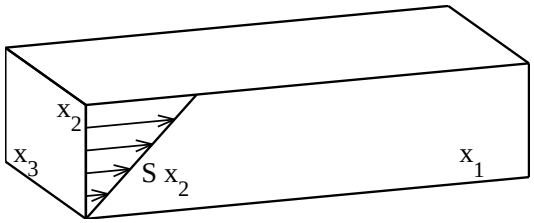

FIGURE 1. Definition of coordinates and of the basic deformation.

by Jiménez *et al.* (2006) in the proceedings of the 2006 CTR summer program, where references can be found to the original publications. The issue is the survival of turbulence over long periods, of the order of many thousand shear times. Simulations up to now have been inconclusive because of their limited Reynolds numbers, but the arguments above suggest that, in any case, the sheared-box approximation might not be very relevant to the long-term evolution of the real flow. More complete models have also been used, taking, for example, into consideration the inhomogeneity of the flow at scales of the order of the disk thickness (e.g. Barranco & Marcus 2005). The results suggest that some form of turbulence may survive for long periods, but they are again limited to relatively low Reynolds numbers by the intrinsically higher complication of the computer codes.

In this report we address the question of whether numerical schemes can be devised to simulate turbulent flows that are not strictly homogeneous, but in which the inhomogeneity is imposed in one direction by boundary conditions that mimic interior planes of the flow, rather than physical walls or other boundaries. Note that the utility of such schemes extends beyond quasi-homogeneous shear flows, or astrophysics. Similar problems appear, for example, in designing off-wall boundary conditions for wall-bounded flows.

In the next section we briefly analyze the available methods for simulating homogeneous sheared flows. In Section 3 we introduce new approximate boundary conditions that can be adapted to model either homogeneous or inhomogeneous cases. These conditions are tested in Section 4 by repeating the simulations by Umurhan & Regev (2004) of sheared homogeneous 2-D turbulence, in the context of accretion disks. Open questions are then summarized.

2. The periodic-box approximation

Most simulations of homogeneous turbulence are based on an analogy with the linearized problem of a small velocity perturbation, $\mathbf{u}$, riding on a uniform shear. Rotation can easily be added by expressing the equations in a rotating frame of reference, but this will not be considered here. In the simple case of incompressible homogeneous shear, the flow satisfies

$$\begin{aligned} [\partial_t + x_2\partial_1]\, u_1 + u_2 - H_1 + \partial_1 p &= \varepsilon\nabla^2 u_1, \\ [\partial_t + x_2\partial_1]\, u_2 - H_2 + \partial_2 p &= \varepsilon\nabla^2 u_2, \\ [\partial_t + x_2\partial_1]\, u_3 - H_3 + \partial_3 p &= \varepsilon\nabla^2 u_3, \\ \partial_j u_j &= 0, \end{aligned} \tag{2.1}$$

where the $H_i = -u_j\partial_j u_i$ are the non-linear advective terms, the kinematic pressure p absorbs the constant fluid density, the subindices refer to the three coordinate directions, and repeated indices imply summation. The flow is assumed to be periodic in the x_1

and x_3 coordinates, and sheared along x_2 (see fig. 1). The equations are normalized with the mean shear rate, S, and with a reference length L. The undisturbed velocity is $\mathbf{U} = [x_2,\, 0,\, 0]$ in the dimensionless variables.

Besides the geometric parameters describing the shape of the simulation domain, the flow depends on the Rossby number,

$$Ro = \frac{u}{SL}, \tag{2.2}$$

where u is a characteristic velocity scale for the fluctuations, and on the Ekman number

$$\varepsilon = \frac{\nu}{SL^2}, \tag{2.3}$$

where ν is the kinematic viscosity. The latter is the inverse of a Reynolds number, and, if L is chosen to be the integral scale of the flow, the Rossby number is the ratio between the time scale S^{-1} of the shear and that of the fluctuations, L/u.

When the gradients of the fluctuations are small with respect to S, or equivalently, when $Ro \ll 1$, the non-linear terms in (2.1) can be neglected with respect to the shear, and the equations become linear and homogeneous. In that "rapid distortion" limit, the solutions to the initial value problem in an unbounded or periodic domain can be expressed as sums of elementary basis functions of the form

$$u_j = \widehat{u}_j(t) \exp\left[\mathrm{i} k_m(t) x_m\right], \tag{2.4}$$

where

$$\begin{aligned} k_1 &= k_1(0) \equiv k_{10}, \\ k_2 &= k_{20} - k_{10} t, \\ k_3 &= k_{30}, \end{aligned} \tag{2.5}$$

which is equivalent to expressing the solutions in the shearing coordinates

$$\begin{aligned} x_1' &= x_1 - S x_2 t, \\ x_2' &= x_2, \\ x_3' &= x_3. \end{aligned} \tag{2.6}$$

In the fully non-linear case, working in the moving frame (2.5) or (2.6) removes from the equations the explicit effect of the shear, and allows periodic boundary conditions to be imposed in the coordinates (2.6),

$$F(x_1',\, x_2',\, x_3') = F(x_1' + n_1 L_1,\, x_2' + n_2 L_2,\, x_3' + n_3 L_3). \tag{2.7}$$

The n_j's are arbitrary integers, the L_j's are the three spatial periodicities, and F is any flow variable. While those boundary conditions are essentially arbitrary, they guarantee the spatial homogeneity of the statistics, and allow the use of spectral numerical methods in the transformed coordinates.

The basic algorithm was introduced by Rogallo (1981), and has been used often since then. He noted that the grid (2.6) becomes progressively skewed with time, and that the flow has to be periodically remeshed to keep the numerical errors in check. Unfortunately, the remeshing results in substantial losses of enstrophy and of energy that degrade the accuracy of the solution, especially for $Ro \ll 1$ (Lee *et al.* 1990).

The problem is sketched in Fig. 2. Assume that the grid is initially orthogonal, and that the wavenumbers of the Fourier expansion in the $(x_1,\, x_2)$ plane are contained in the

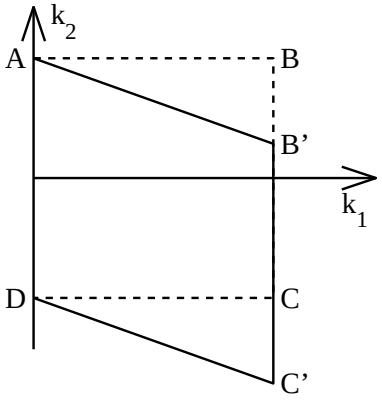

FIGURE 2. Deformation of the wavenumber domain under the effect of the shear.

rectangle ABCD. After some time, the transformation (2.5) deforms the wavenumber domain to AB'C'D. Note that, because of the periodicity of the discrete Fourier transform, the wavenumber triangle DCC' is reproduced in ABB', but that the interpretations of the modes in the two locations are different, especially when derivatives are computed from the expansion (2.4). After some time, the expansion becomes increasingly unbalanced. Remeshing to the original orthogonal grid restores the interpretation of the modes in both triangles, in effect copying DCC' into ABB'. The effective wavenumbers, and therefore the velocity gradients, decrease in this operation, leading to the characteristic loss of enstrophy during remeshing. Rogallo (1981) interpreted the relabeling of the wavenumbers as aliasing, and his original algorithm avoids it by padding with zeros the Fourier expansion in k_2 before the pseudospectral interpolation step.

In fact, it is clear from Fig. 2 that the problem is not so much with discarding the information in DCC', where viscosity should have damped the flow, as with the arbitrary information injected in ABB' during remeshing. The deformation due to the shear continuously injects new modes into the computational domain from a spectral "upstream" reservoir, but their information is unknown to the numerical algorithm. Both zeroing the incoming modes, as in the de-aliased remeshing, or substituting them with information from DCC', are unjustified. Eventually, the modes arbitrarily created in ABB' return to some equilibrium value under the effect of non-linearity, but the remeshing amounts to a periodic resetting of the initial conditions that becomes more severe as the remeshing period increases. Brucker *et al.* (2007) recently proposed an alternative method that, in essence, remeshes every time step, and which minimizes the error by reducing the number of modes for which arbitrary values are assigned, but the problem persists. Perhaps the only solution is to adjust the grid resolution so that the energy and the enstrophy in the modes crossing AB and DC by the effect of the shear are negligible.

2.1. *Sliding boundary conditions*

A different approach was taken by Baron (1982), and later by Gerz *et al.* (1989). If the x_2 direction is not treated spectrally, the boundary conditions (2.7) need only be applied at the boundaries themselves,

$$F(x_1,\, L_2,\, x_3) = F(x_1 - StL_2 + n_1L_1,\, 0,\, x_3 + n_3L_3). \tag{2.8}$$

Note that there are in (2.8) no direct assumptions about the form of the solution outside the domain $x_2 = (0,\, L_2)$, but that periodic solutions of the form $F(x_1',\, x_2', x_3')$ satisfy both (2.8) and (2.7), so that the two boundary conditions can be considered equivalent.

Although (2.8) was originally formulated for fully finite-difference codes, it is most easily implemented when the two directions normal to the shear are treated spectrally

$$F(x_1,\, x_2,\, x_3) = \widehat{F}(k_1,\, x_2,\, k_3) \exp\left[\mathrm{i}\,(k_1 x_1 + k_3 x_3)\right]. \tag{2.9}$$

In that case, the Fourier components of the flow variables satisfy

$$\widehat{F}(k_1,\, L_2,\, k_3) = \widehat{F}(k_1,\, 0,\, k_3)\, \exp(-\mathrm{i}Stk_1L_2), \tag{2.10}$$

and the finite-difference operators in the x_2 direction retain their band structure, with at most a few off-diagonal elements added at the boundary lines.

3. The generation of interior boundaries

While the sliding boundary conditions discussed in Section 2.1 are equivalent to the periodic-box formulation in Section 2, they are only easy to implement when the desired relation between the two boundaries is linear. Otherwise the transformation between the Fourier coefficients at the two boundaries is not local in wavenumber space, and the problem becomes fully coupled. This makes the introduction of tailored flow inhomogeneity difficult to implement. Think, for example, of a problem in which the goal is to capture a vertical gradient of the integral scale of the turbulence.

In those cases, it is easier to implement the boundary conditions explicitly. For example, the velocities at the top boundary at time t can be copied from the bottom boundary in the previous time step, $t - \Delta t$,

$$\begin{aligned} \widehat{F}(L_2,\, t) &= \widehat{F}(0,\, t - \Delta t)\, \exp(-\mathrm{i}Stk_1L_2). \\ \widehat{F}(0,\, t) &= \widehat{F}(L_2,\, t - \Delta t)\, \exp(\mathrm{i}Stk_1L_2), \end{aligned} \tag{3.1}$$

where the dependence of $\widehat{F}$ on the two Fourier wavenumbers has not been included to simplify the notation. Note that the explicit time dependence of $\widehat{F}$ refers only to its "slow" evolution due to the non-linear terms, while the "fast" translation due to the shear has been included in the phase factor. Note also that (3.1) differs from (2.7) or (2.8) by an amount $O(\Delta t)$, although it is difficult to justify which of the two flows should be considered "correct". On the other hand, the explicit character of (3.1) allows arbitrary transformations to be applied to $\widehat{F}(t - \Delta t)$ before it is used as a template for $\widehat{F}(t)$, with little extra work.

Unfortunately, a brief consideration shows that (3.1) is not a good boundary condition. Since the top boundary is a translated version of the bottom one in the previous step, and since it also acts as the template for the bottom boundary in the next step, the result of (3.1) is that the flow is driven by two sliding copies of the two initial boundary planes. If the two planes have been chosen equal, the effect is just to drive the flow between two sliding "walls" with prescribed tangential and normal velocities. If they are chosen differently, the initial conditions switch between the two boundary planes in alternating time steps.

One solution is to use as boundary templates two interior planes, instead of the boundaries themselves. Referring to Fig. 3 for the geometry, the new conditions are

$$\widehat{F}(L_2,\, t) = \widehat{F}(L_A,\, t - \Delta t)\, \exp\left[\mathrm{i}Stk_1(L_A - L_2)\right].$$

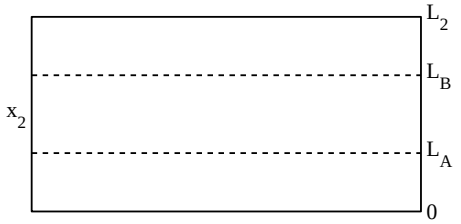

FIGURE 3. Interior planes used to generate the boundary conditions.

$$\widehat{F}(0,\,t) = \widehat{F}(L_B,\,t-\Delta t)\,\exp\left[\mathrm{i}Stk_1L_B\right]. \tag{3.2}$$

The use of internal planes to act as boundary templates is conceptually similar to the method used by Lund *et al.* (1998) to generate turbulent inflow conditions. In the present case both boundaries act as inflow and outflow, although the main difficulties are in those parts acting as inflows. Information on the incoming flow has to be synthesized, and the idea is to derive that information from the simulation itself. Although the top boundary is still essentially copying its information from the bottom one, and vice versa, the accommodation layers $x_2 = (0,\,L_A)$ and $x_2 = (L_B,\,L_2)$ act as buffers in which the information injected at the boundary loses its coherence, and becomes "healthy" turbulence.

In the case of Fig. 3 the periodicity is imposed both between the planes $x_2 = (0,\,L_B)$ and between $x_2 = (L_A,\,L_2)$, so that the two shifted–periodic simulations are being run simultaneously. However, the two accommodation layers $(0,\,L_A)$ and $(L_B,\,L_2)$ have essentially identical boundary conditions, and should also be identical, except for the shift. The two overlapping simulations are therefore equivalent to each other up to $O(\Delta t)$. Note however that the same would not be true if the template planes had been transformed differently before being applied to the boundaries. For example, if a length-scale gradient had been imposed, the two overlapping simulations would correspond to different scale ranges. In that case there would no requirement of periodicity, and the whole domain could be considered as a single simulation.

4. Numerical experiments

To test the feasibility of the boundary conditions described above, we have implemented them for the 2-D homogeneous flow studied by Umurhan & Regev (2004) as a model for the survival of turbulence in accretion disks. Rotation has no effect in two dimensions, except for modifying the pressure, and the problem reduces to the decay of initially isotropic 2-D initial conditions in a shear.

The equations can be written in terms of a perturbation vorticity and stream function, ω and ψ, as

$$(\partial_t + Sx_2\partial_1)\omega + u_j\partial_j\omega = \varepsilon\nabla^2\omega, \tag{4.1}$$

where

$$\omega = -\nabla^2\psi, \quad \text{and} \quad \mathbf{u} = (\partial_2,\,-\partial_1)\psi. \tag{4.2}$$

The flow is assumed to be periodic in the x_1 direction, with wavelength L_1, and should ideally satisfy the sliding periodic boundary conditions (2.8) in the domain $x_2 = (L_A,\,L_2)$, where $L_2 - L_A \equiv H$. In practice, the boundary conditions are applied using for ψ, ω, and for the mean profile of the horizontal velocity, a generalized version of the explicit

formulation (3.2). The algorithm keeps track of the mean translation of each of the two boundaries and reference planes, computed as

$$\partial_t X_j = \langle U_1(x_1, L_j, t)\rangle, \tag{4.3}$$

where U_1 includes the perturbation velocity and the shear, and the averages $\langle\,\rangle$ are defined over lines of constant x_2. The boundary conditions are then

$$\begin{aligned}\widehat{F}(L_2, t) &= \widehat{F}(L_A, t-\Delta t)\,\exp\left[\mathrm{i}k_1(X_A - X_2)\right].\\ \widehat{F}(0, t) &= \widehat{F}(L_B, t-\Delta t)\,\exp[\mathrm{i}k_1(X_B - X_0)].\end{aligned} \tag{4.4}$$

The code uses Fourier expansions in the x_1 direction, and compact finite differences in x_2 with a seven-point stencil over a uniform grid. Of the thirteen coefficients available for each interior point of the finite difference scheme, seven are used to impose sixth-order consistency, and the rest enforce spectral-like resolution at three wavenumbers ($k_2\Delta x_2/\pi = 0.5, 0.7, 0.9$) (Lele 1992). The three points near each boundary do not support full resolution. It was decided to respect in them the bandwidth of the two finite-difference matrices, and to reduce progressively both the consistency order and the number of spectral points ($N_{sp} = 3$, 2 and 2). After considerable experimentation, this solution was found to improve the resolution properties near the boundaries, even if the last boundary point is only consistent to second order.

The mean quantities over x_1, which correspond to Fourier components with $k_1 = 0$, are best treated in terms of velocities, instead of vorticity, because they involve the effect of the pressure gradient. It follows from continuity and from the vertical momentum equation that

$$\partial_2\langle u_2\rangle = 0, \tag{4.5}$$

$$\partial_t\langle u_2\rangle + \partial_2\langle u_2^2 + p - \varepsilon\partial_2 u_2\rangle = 0. \tag{4.6}$$

It follows from (4.5) that the mean vertical velocity is constant, although possibly a function of time, while (4.6) shows that that constant can be chosen arbitrarily by introducing a pressure gradient in the x_2 direction. In any case, because the horizontal averages are independent of x_1, the mean horizontal pressure gradient is independent of x_2. The horizontal momentum equation then reads

$$\partial_t\langle u_1\rangle + \partial_2\langle u_1u_2 - \varepsilon\partial_2 u_1\rangle + \langle\partial_1 p\rangle = 0. \tag{4.7}$$

Integrating over the vertical periodicity domain, and recalling that the horizontal averages remain periodic despite the horizontal shift, the mean volume flux satisfies

$$\partial_t\int_0^H \langle u_1\rangle\,\mathrm{d}x_2 = -H\langle\partial_1 p\rangle. \tag{4.8}$$

In systems with a velocity reference, such as a no-slip wall, this equation results in the classical dichotomy between simulations at constant mass flux and those at constant pressure gradient. In the present case the two are strictly equivalent. The incompressible Navier–Stokes equations are invariant to a uniform, possibly time-dependent, acceleration of the frame of reference. Its only effect is to create a variable gradient of the "hydrostatic" pressure. In the absence of a velocity reference, the fluctuations of the mean velocity and of the mean pressure gradient are interchangeable. The simulation can be performed in either mode, and later translated to the other one if required. In the present simulations, we have adopted for numerical convenience the conventions

$$\langle u_2\rangle = 0, \quad \text{and} \quad \langle\partial_1 p\rangle = 0. \tag{4.9}$$

In the case of periodic sheared turbulence, another interesting consequence of the boundary conditions is that

$$\partial_t \left[\langle u_1 \rangle(H) - \langle u_1 \rangle(0)\right] = 0, \tag{4.10}$$

so that, once the velocity difference is defined by the initial conditions, it remains constant. This provides a useful test for the accuracy with which true periodicity is enforced.

All our simulations were performed in boxes with $H = 2$, and $L_1 = 2\pi$. Time was normalized with the shear rate, whenever appropriate, so that either $S = 1$ or $S = 0$. The latter was used in some preliminary unsheared cases, not presented here due to space limitations. The interior planes used as templates for the boundary conditions were located symmetrically with respect to the box with $L_A/L_2 = 0.1$, although some experimentation was performed with this parameter. Integral quantities, such as mean energy or enstrophy, are always given in the layer $x_2 = (L_A, L_2)$. The other two parameters tested were the initial root-mean-squared (r.m.s.) velocity magnitude u', and the wavenumber k_0 of the initial spectral peak. The tests were initialized with nominally isotropic turbulence with random phases, and with a sharp enstrophy spectrum behaving as $k^{3/2}$ for wavenumbers $k \ll k_0$, and as k^{-7} for $k \gg k_0$.

Integrating (4.1) over the computational domain shows that the r.m.s. vorticity can only decrease under the effect of viscosity, so that all initial conditions eventually decay to a uniform shear over viscous time scales. The temporal derivative of the energy, on the other hand, satisfies

$$\partial_t(u'^2) = -2S\langle u_1 u_2 \rangle - 2\varepsilon |\nabla \mathbf{u}|^2, \tag{4.11}$$

which can have either sign, depending on the magnitude of the average tangential Reynolds stress $\tau_{12} = -\langle u_1 u_2 \rangle$. Equation (4.11) also applies to the 3-D case, and shows that turbulence can only survive if the "eddy viscosity" of the flow, τ_{12}/S, is positive.

Umurhan & Regev (2004) noted that, while the decay of the enstrophy was uniform in their experiments, the energy underwent repeated periods of transient growth and decay. They showed that those episodes followed closely the transient linear behavior of a particular set of initial conditions in the rapid distortion limit. They speculated that a similar process could occur in the 3-D case, with non-linearity generating the necessary initial conditions for new growth episodes from the decay products of previous ones. It was difficult to go much further in the interpretation of their results, because they chose their Reynolds numbers to provide very long decay times, but very little in the way of clean structures. Our goal in the next section will be to reproduce their results, partly to clarify the transient growth mechanism, but mostly to test our boundary conditions.

4.1. *Sheared turbulence*

Equations (4.1) and (4.2), with $S = 1$, were allowed to evolve from the nominally isotropic initial vorticity distributions described above. The initial length scale turned out to be important, and a parametric study was undertaken in the range $k_0 H = (2, 30)$. The evolution becomes roughly independent of k_0 whenever $k_0 H > 8$, which corresponds to more than roughly one initial vortex across the short dimension of the box. As seen in Fig. 5, the flow evolves into coherent vortices, as it does in the unsheared case (McWilliams 1984), but initial conditions without at least one initial vortex across the box height are unable to create such structures. The results in this section are computed with $k_0 H = 20$, corresponding to about three vortices across the shortest box dimension, but similar ones shown are obtained for $k_0 H \in (10, 30)$.

The evolution of the energy and of the enstrophy are shown in Fig. 4(a). The enstrophy

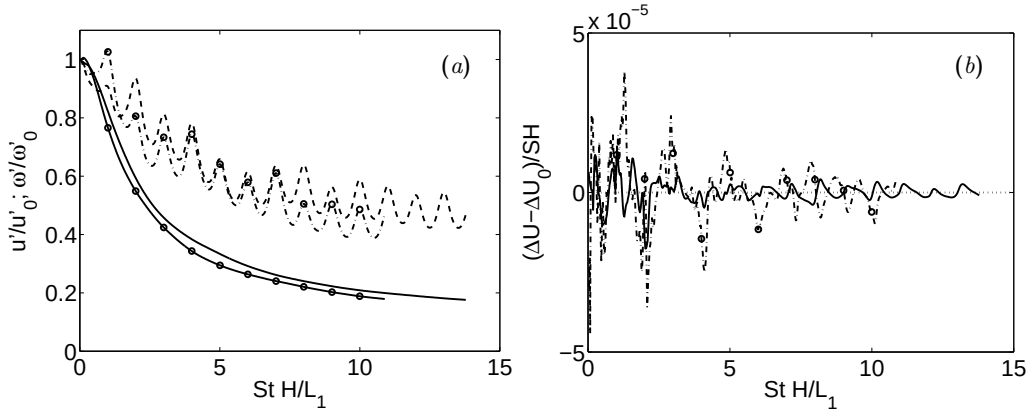

FIGURE 4. Results from two simulations of decaying sheared turbulence. (*a*) Evolution of the r.m.s. vorticity (———), and of the r.m.s. velocity magnitude (- - - - and —·—). The resolution is 576×193 collocation points for a box $H \times L_1 = 2 \times 2\pi$, $SH^2/\nu = 1.6 \times 10^4$, and $S = 1$. The lines without symbols have $u_0'/SL = 0.025$; those with symbols have $u_0'/SL = 0.05$. Each line is the average of eight simulations. (*b*) Evolution of the mean velocity difference between the top boundary and its template plane.

decays monotonically, as it should in a periodic box, but the decay of the energy is oscillatory, as in Umurhan & Regev (2004). Note that the two simulations in the figure decay at roughly the same rate, even if their initial Rossby numbers differ by a factor of two. This shows that the time scale of the decay is set by the shear – although with a weaker influence of the Ekman number – instead of by the magnitude of the initial velocity perturbations. This agrees with the linearized rapid distortion theory. The mean velocity difference is shown in Fig. 4(*b*), and remains very nearly constant, as required by (4.10), showing that the boundary conditions truly enforce periodicity. It can actually be shown that most of the observed deviations are due to the initial conditions, which were not chosen periodic in x_2.

Some instantaneous vorticity fields are shown in Fig. 5. After a while, the shear tilts the initial structures, and vortices counter-rotating with the shear are shredded away, while co-rotating ones (dark in the figure) survive. This has been observed in all previous simulations of this flow (e.g. Godon & Livio 1999). The vorticity of the counter-rotating cyclonic vortices subtracts from the mean vorticity of the shear, while that of the co-rotating anticyclonic ones add to it. Anticyclones are in effect stronger than cyclones.

The most interesting feature of the simulations are the oscillations superimposed to the slow decay of the kinetic energy. Umurhan & Regev (2004) explained them as the result of transient growth in the linearized rapid-distortion representation of the flow. Basically, Fourier modes that are originally tilted to the left rotate with the shear, and reach their maximum amplitudes when they are oriented vertically. Later, as the shear keeps tilting them to the right, their energy decreases. Non-linearity is then assumed to introduce new perturbations with the right orientation, re-initiating the cycle. Inspection of the flowfields in Fig. 5 suggests that the same mechanism can be expressed in a somewhat simpler way, which is also fully non-linear and requires no especial assumptions to be re-initialized. We have already seen that the flow evolves quickly into a few vortices of the same sign, which are then essentially advected by the mean shear. However, since the flow is periodic in both x_1 and x_2 the true picture is a series of rows of vortices, periodic in x_1 with wavelength L_1. These rows are separated in x_2 by a distance H, and slide

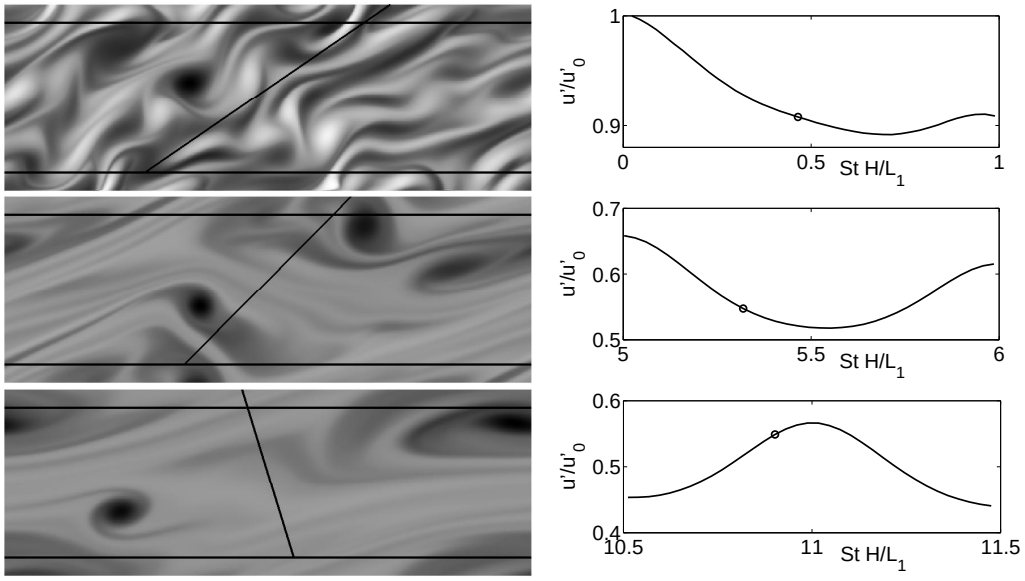

FIGURE 5. Left figures are vorticity maps from the shear simulation in Fig. 4 with $u'_0/SL = 0.025$. From top to bottom, $StH/L_1 = 0.5$, 5.3, 10.9. The horizontal lines are the template planes, and the diagonal ones join congruent points of the boundary conditions. Right figures are the evolution of the total energy, with the symbols marking the time of each snapshot.

past each other with a relative velocity SH. They are vertically aligned at integer values of StH/L_1, and it is at those times when the vortices are closest to each other. That is when the kinetic energy of a set of vortices of the same sign is maximum (Batchelor 1967, Section 7.3), which is why the energy increases. As the rows keep sliding past each other the vortices separate, and the energy decreases until they again become aligned in the next cycle.

Note that the moment of maximum energy is determined by the offset in the boundary conditions (4.4), not by the structure of the flow. This is why all our simulations burst synchronously, and why the oscillations survive even after averaging over the eight cases used for each curve in Fig. 4. The symbols used to mark one of simulations in that figure are at integer dimensionless times, and roughly correspond to the energy maxima. In the right-hand side of Fig. 5 we have included the evolution of the energy in a time interval around each snapshot. It is clear that the only case in which the energy is close to a maximum is the bottom one, for which the two boundary conditions are almost in phase. This leads to the closest approach among the different copies of the large vortex to the right of the snapshot, and therefore to the energy maximum. Note that individual simulations undergo smaller-scale energy oscillations when different vortices in the box approach each other. Those variations are averaged out of the mean traces in Fig. 4, and only the basic cycle remains.

The argument can be made quantitative. Approximating the flow by a series of rows of point vortices of circulation γ, and defining a complex variable $z = x_1 + \mathrm{i}x_2$, the complex velocity is given by

$$u_1 - \mathrm{i}u_2 = \frac{\gamma}{2\mathrm{i}L_1} \sum_{m=-\infty}^{\infty} \cot \pi \frac{z + m\zeta + \mathrm{i}mH}{L_1}, \tag{4.12}$$

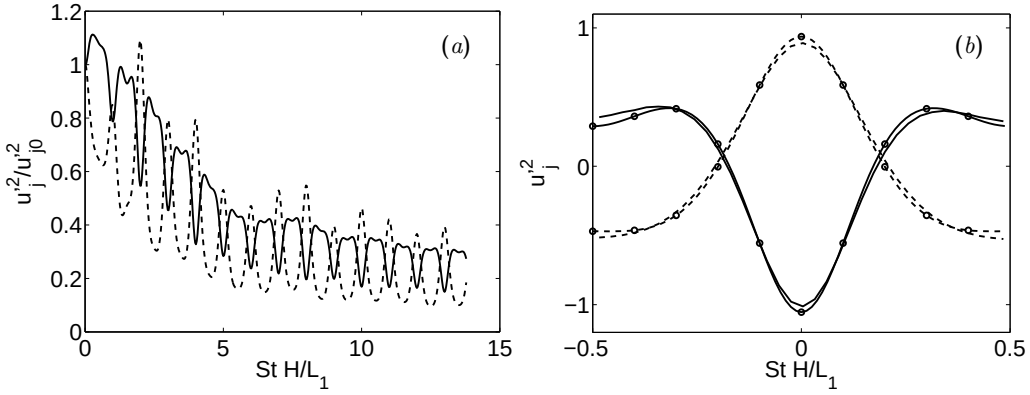

FIGURE 6. Mean-squared fluctuations of the individual velocity components. (a) From the simulation in Fig. 4 with $u_0'/SL = 0.025$. ——— , $u_1'^2$; - - - - , $u_2'^2$. (b) Comparison of the period around $t\Delta U/L_1 = 10$ with the results of (4.12) (with symbols).

where $\zeta \in (-L_1/2,\, L_1/2)$ is the horizontal offset among contiguous rows. The series converges rapidly with $|m|$ because the velocity field induced by each row decays exponentially with x_2. Separating the two velocity components, and subtracting the infinite self-energy of an individual point vortex, we obtain numerically the temporal evolution of the two kinetic energies. They are compared in Fig. 6(b) with a corresponding period of the simulations. Note that the magnitudes and origins of the energies, which depend on the details of the vortex cores, have been adjusted for the comparison, but that there are no adjustable parameters in either the scaling or the phase of the time.

Note that the overtaking process just described is periodic, so that there is no net energy generation over a full cycle. Equation (4.11) then implies that the flow cannot create any average tangential Reynolds stress. This is an important point in astrophysical applications, where what is usually required is a mean momentum transfer among the different disk radii. Note however that this conclusion could be different in three dimensions, where the vortex conjunction could extract a non-zero amount of energy from the mean shear.

5. Discussion

We have presented a new set of boundary conditions that can be used in the simulation of shear flows away from walls. They have been tested by reproducing previous simulations of 2-D sheared turbulence, which had been performed in the context of astrophysical accretion disks. The results agree qualitatively, and show that the required spacial periodicity of the resulting flow is achieved. We have also proposed a simpler, fully non-linear, interpretation of the transient energy growth previously observed in this flow, but we have noted that, at least in the 2-D context, it does not result in any mean momentum transfer.

The new boundary conditions can easily be adapted to cases in which the relation between the two flow boundaries is more general than a simple homogeneous shear. Both that extension, and the implementation in 3-D flows, are currently under way.

Acknowledgments

This work was supported in part by the Advanced Simulation and Computing program of the Department of Energy, and by grant TRA2006-08226 of the Spanish CICYT. The author is grateful to Y. Mizuno for his careful critique of an earlier version of this manuscript.

REFERENCES

Baron, F. 1982 Macro-simulation tridimensionelle d'écoulements turbulents cisaillés. Ph.D. thesis, Université Pierre et Marie Curie.

Barranco, J. & Marcus, P. 2005 Three-dimensional vortices in stratified protoplanetary disks. *Astrophys. J.* **623**, 1157–1170.

Batchelor, G. 1967 *An introduction to fluid dynamics*. Cambridge: Cambridge University Press.

Brucker, K. A., Isaza, J., Vaithianathan, T. & Collins, L. 2007 Efficient algorithm for simulating homogeneous turbulent shear flows without remeshing. *J. Comput. Phys.* **225**, 20–32.

Champagne, F., Harris, V. & Corrsin, S. 1970 Experiments on nearly homogeneous turbulent shear flow. *J. Fluid Mech.* **41**, 81–139.

Gerz, T., Schumann, U. & Elgobashi, S. 1989 Direct numerical simulation of stratified homogeneous turbulent shear flows. *J. Fluid Mech.* **200**, 563–594.

Godon, P. & Livio, M. 1999 Vortices in protoplanetary disks. *Astrophys. J.* **523**, 350–356.

Jiménez, J., Kassinos, S. & Wray, A. 2006 Analysis of some preliminary simulations of Keplerian turbulence. In *Proc. of the CTR Summer Prog.*, pp. 5–18. Stanford University.

Lee, M. J., Kim, J. & Moin, P. 1990 Structure of turbulence at high shear rates. *J. Fluid Mech.* **216**, 561–583.

Lele, S. 1992 Compact finite difference schemes with spectral-like resolution. *J. Computat. Phys.* **103**, 16–42.

Lund, T. S., Wu, X. & Squires, K. 1998 Generation of turbulent inflow data for spatially-developing boundary layer simulations. *J. Computat. Phys.* **140**, 233–258.

McWilliams, J. C. 1984 The emergence of isolated coherent vortices in turbulent flow. *J. Fluid Mech.* **146**, 21–43.

Pumir, A. 1996 Turbulence in homogeneous shear flows. *Phys. Fluids* **8**, 3112–3127.

Rogallo, R. S. 1981 Numerical experiments in homogeneous turbulence. Tech. Memo 81315. NASA.

Tavoularis, S. & Karnik, U. 1989 Further experiments on the evolution of turbulent stresses in uniformly sheared turbulence. *J. Fluid Mech.* **204**, 457–478.

Umurhan, O. M. & Regev, O. 2004 Hydrodynamic stability of rotationally supported flows: linear and nonlinear 2D shearing box results. *Astron. Astrophys.* **427**, 855–872.